The Journal of Chemical Physics

RESEARCH ARTICLE | APRIL 25 2024

Photodissociation dynamics of SO_2 via the $\tilde{G}^1B_1$ state: The $O(^1D_2)$ and $O(^1S_0)$ product channels

Yucheng Wu; Jitao Sun ; Zhenxing Li ; Zhaoxue Zhang; Zijie Luo; Yao Chang ; Guorong Wu ; Weiqing Zhang ; Shengrui Yu ; Kaijun Yuan ; Xueming Yang

Check for updates

J. Chem. Phys. 160, 164311 (2024)
https://doi.org/10.1063/5.0208090

View Online
Export Citation

Articles You May Be Interested In

Photodissociation dynamics of SO_2 between 193 and 201 nm

J. Chem. Phys. (July 2023)

Spectroscopic snapshot for neutral water nonamer $(H_2O)_9$: Adding a H_2O onto a hydrogen bond-unbroken edge of $(H_2O)_8$

J. Chem. Phys. (January 2023)

Two-color visible/vacuum ultraviolet photoelectron imaging dynamics of Br 2

J. Chem. Phys. (October 2006)

26 September 2024 02:50:31

Nanotechnology & Materials Science
Optics & Photonics
Impedance Analysis
Scanning Probe Microscopy
Sensors
Failure Analysis & Semiconductors

Unlock the Full Spectrum.
From DC to 8.5 GHz.
Your Application. Measured.
Find out more
Zurich Instruments

AIP Publishing

The Journal of Chemical Physics ARTICLE pubs.aip.org/aip/jcp

Photodissociation dynamics of SO_2 via the $\tilde{G}^1B_1$ state: The $O(^1D_2)$ and $O(^1S_0)$ product channels

Cite as: J. Chem. Phys. 160, 164311 (2024); doi: 10.1063/5.0208090
Submitted: 13 March 2024 • Accepted: 9 April 2024 •
Published Online: 25 April 2024

View Online Export Citation CrossMark

Yucheng Wu,[1,2] Jitao Sun,[1,2] Zhenxing Li,[1] Zhaoxue Zhang,[1] Zijie Luo,[1] Yao Chang,[1,a)] Guorong Wu,[1] Weiqing Zhang,[1] Shengrui Yu,[3,a)] Kaijun Yuan,[1,2,4,a)] and Xueming Yang[1,4,5]

AFFILIATIONS

[1] State Key Laboratory of Molecular Reaction Dynamics and Dalian Coherent Light Source, Dalian Institute of Chemical Physics, Chinese Academy of Sciences, 457 Zhongshan Road, Dalian 116023, China
[2] University of Chinese Academy of Sciences, Beijing 100049, China
[3] Hangzhou Institute of Advanced Studies, Zhejiang Normal University, 1108 Gengwen Road, Hangzhou, Zhejiang 311231, China
[4] Hefei National Laboratory, Hefei 230088, China
[5] Department of Chemistry and Center for Advanced Light Source Research, College of Science, Southern University of Science and Technology, Shenzhen 518055, China

[a)] **Authors to whom correspondence should be addressed:** cy2015@mail.ustc.edu.cn; sryu@zjnu.cn; and kjyuan@dicp.ac.cn

ABSTRACT

Produced by both nature and human activities, sulfur dioxide (SO_2) is an important species in the earth's atmosphere. SO_2 has also been found in the atmospheres of other planets and satellites in the solar system. The photoabsorption cross sections and photodissociation of SO_2 have been studied for several decades. In this paper, we reported the experimental results for photodissociation dynamics of SO_2 via the $\tilde{G}^1B_1$ state. By analyzing the images from the time-sliced velocity map ion imaging method, the vibrational state population distributions and anisotropy parameters were obtained for the $O(^1D_2) + SO(X^3\Sigma^-, a^1\Delta, b^1\Sigma^+)$ and $O(^1S_0) + SO(X^3\Sigma^-)$ channels, and the branching ratios for the channels $O(^1D_2) + SO(X^3\Sigma^-)$, $O(^1D_2) + SO(a^1\Delta)$, and $O(^1D_2) + SO(b^1\Sigma^+)$ were determined to be ~0.3, ~0.6, and ~0.1, respectively. The SO products were dominant in electronically and rovibrationally excited states, which may have yet unrecognized roles in the upper planetary atmosphere.

Published under an exclusive license by AIP Publishing. https://doi.org/10.1063/5.0208090

26 September 2024 02:50:31

I. INTRODUCTION

The SO_2 molecule is of great interest for a variety of scientific disciplines and for a range of different reasons. The photodissociation and absorption cross sections of SO_2 have consequently been studied for many years, not only in experiments[1–13] but also in theoretical calculations.[14–35] Since its presence as a pollutant in the earth's atmosphere leads to acid rain, SO_2 is extremely important in environmental and atmospheric chemistry. SO_2 enters the atmosphere through various processes, including natural processes (e.g., volcanic eruptions, forest fires, and biological decay) and human activity (e.g., burning of fossil fuels and chemical engineering). Furthermore, SO_2 has been widely identified in the interstellar medium (ISM),[36–40] as well as in the atmosphere of Venus[41,42] and Io,[43–46] due to its unusually strong spectroscopic signature. In fact, it is so strong that the researchers are often faced with the problem of having to "weed out" the SO_2 signature from spectral data, in order to correctly identify other molecular species that are also present. For this purpose, accurate and comprehensive spectral lines of SO_2 have been studied,[10–13,19–25,47–51] especially for different isotopologues.[26–29,52] Simultaneously, it was found that the SO_2 molecules act an important role in a marked sulfur isotope mass independent fractionation (S-MIF) effect,[53–56] which timely coincided with the great oxidation event,[36,54] so the scientists pay more and more attention to the photodissociation of SO_2.[3–7,16,57–60]

As shown in Fig. 1, the absorption spectrum of electronically excited SO_2 exhibits many structures in the UV and vacuum ultraviolet (VUV) regions, and the range from 220 to 390 nm is not displayed here due to its nature of non-dissociation. In the near UV region, there are three absorption bands for SO_2.[47] The first band

Published under an exclusive license by AIP Publishing

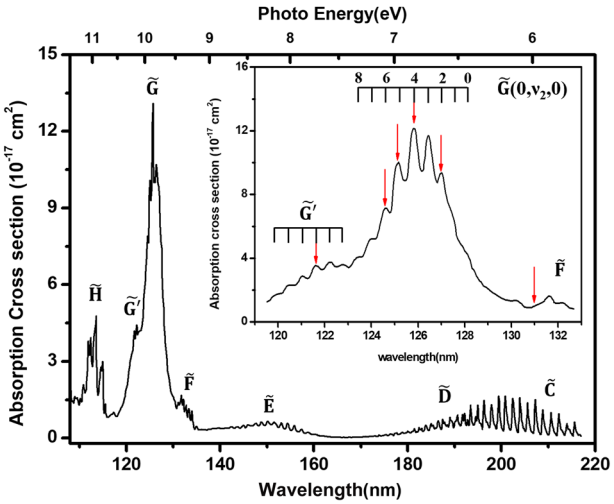

FIG. 1. Absorption spectrum of SO_2 in the vacuum ultraviolet region (the data adapted from Ref. 47). The inset shows the wavelength region studied in this experiment, in which the photolysis excitation wavelengths are marked by the red downward arrows.

with extremely weak intensity and ranging from 390 to 340 nm is assigned to the spin-forbidden $\tilde{a}^3B_1 \leftarrow \tilde{X}^1A_1$ transition. The stronger second band from 340 to 260 nm is attributed to combined $\tilde{A}^1B_1 \leftarrow \tilde{X}^1A_1$ and $\tilde{B}^1A_2 \leftarrow \tilde{X}^1A_1$ transitions. The $\tilde{B}^1A_2 \leftarrow \tilde{X}^1A_1$ transition is dipole forbidden but becomes allowed thanks to the strong non-adiabatic couplings between the $\tilde{B}^1A_2$ and $\tilde{A}^1B_1$ states. Known as the Clements bands,[61] the complex vibrational progression in the second band is difficult to assign due to the nonadiabatic mixing. The third band located in the 240–180 nm region is assigned to the $\tilde{C}^1B_2/\tilde{D}^1A_1 \leftarrow \tilde{X}^1A_1$ transition, which is the most complex and has been heavily investigated by several groups due to its strong relation with the S-MIF.[23,28,60] In its high energy wing (<218 nm), the molecule is predissociative to $O(^3P) + SO(X^3\Sigma^-)^1$. The vibrational structure in this absorption band has also been calculated quantum mechanically and is reasonably regular and assignable.[18–20,26] About the dissociation happened on this state, there are three disputable dissociation mechanisms: internal conversion to quasi-bound continuum levels of the $\tilde{X}$ ground state,[32] intersystem crossing onto the repulsive 2^3A_1 surface, and a crossing with the $\tilde{D}$ state,[16] resulting in the $O(^3P) + SO(X^3\Sigma^-)$ channel.

At shorter wavelengths, another absorption band appears in the range of ~138–162 nm, shown a well-defined progression in the low energy region, followed by more complex structures, which is assigned to the $\tilde{E}^1A_2$ state. Whether they all relate to the same electronic origin is unclear due to less attention paid by scientists. The next range of ~130–135 nm belongs to the first Rydberg state ($\tilde{F}^1A_1$) converging to the SO_2^+ $3s\tilde{X}$ state. From this state, Svoboda *et al.*[62] observed a rapid decay with a time constant of ~80 fs in both photo-ion and photoelectron yields. The observed time-dependent photoelectron angular distributions were consistent with the $\tilde{F}$ band corresponding to a Rydberg state of dominant *s* character. At around 120 nm, the vibrational progression has the maximal absorption cross section along the whole spectral region, which is assigned to the $\tilde{G}$ Rydberg states ($4p_x\tilde{X}^+$),[63] and is selected as the research object in this work. In the region of wavelength shorter than 120 nm, a series of vibrational progressions are ascribed to the $\tilde{H}$–$\tilde{K}$ Rydberg states, not tired in words here.

Although a series of studies have been performed to enhance our understanding of the photodissociation mechanism of SO_2, primarily due to its significance in the atmospheric sulfur cycle and its application as a test system for chemical physics, the majority of previous studies only concentrated on the photodissociation dynamics of SO_2 via the $\tilde{C}$ state. In contrast, the dissociation processes occurred on the higher potential energy surfaces (PESs) have received few investigations so far. In this paper, we reported the experimental results of SO_2 photodissociation via the $\tilde{G}$ state. By analyzing the images from the time-sliced velocity map ion imaging experiments, the vibrational state population distributions and anisotropy parameters were obtained for the $O(^1D_2) + SO(X^3\Sigma^-, a^1\Delta, b^1\Sigma^+)$ and $O(^1S_0) + SO(X^3\Sigma^-)$ channels, as well as the fraction ratios of $SO(X^3\Sigma^-, a^1\Delta, b^1\Sigma^+)$ products.

II. EXPERIMENTAL METHODS

The experimental setup of the VUV pump–VUV probe time-sliced velocity map ion imaging (TSVMI) apparatus has been described previously,[64–67] but combined with the resonant sum-frequency four-wave mixing method,[68–70] as shown in Fig. 2. Briefly, the apparatus consisted of two independently tunable VUV lasers: one was generated by the free electron laser (denoted as VUV-FEL) from the Dalian Coherent Light Source (DCLS)[71] acting as the photolysis laser, and the other was produced by the resonant sum-frequency four-wave mixing (denoted as VUV-SFWM) method from the table-top lasers and served as the probe laser. All the lasers had a horizontal polarization vector, which was parallel to the front face of the microchannel plate (MCP) detector.

The VUV-FEL ran in the high gain harmonic generation (HGHG) mode[72] and was able to yield VUV laser beam with pulse energies >200 μJ, duration ~1.5 ps, and a repetition rate of 10 Hz at any user selected wavelength in the range of $50 \le \lambda \le 150$ nm. The typical spectral bandwidths were in the range of 30–70 cm^{-1}.

The $O(^1D_2)$ atoms produced in the VUV photodissociation of SO_2 were ionized by a VUV-SFWM laser via the autoionization line at 92.201 nm ($O^*[2s^22p^3(^2D^\circ_{3/2})3d\ (^1F^\circ_3)] \leftarrow O(^1D_2)$).[73] The 92.201 nm light came from the resonant sum-frequency ($2\omega_1 + \omega_2$) four-wave mixing by using Xe as the nonlinear medium, in which ω_1 was set at the two-photon resonant frequency for the Xe $[5p^5(^2P^\circ_{1/2})6p\ ^2[^1/_2]_0 \leftarrow 5p^6\ ^1S_0]$ transition, i.e., 222.568 nm, and ω_2 was scanned back and forth equally around 537.671 nm to cover the Doppler profile. The Xe gas was sprayed into a T-shape tube by the general valve with a bore diameter of 1 mm, in which the SFWM process occurred when the fundamental laser and Xe gas arrived synchronously. The laser light at $\lambda = 222.568$ nm (~1 mJ) was obtained by tripling the output of a 532 nm (Nd:YAG laser, Continuum PL-9030) pumped dye laser (Sirah, PESC-G-18) operating at $\lambda \sim 667$ nm. The 355 nm output of the same Nd:YAG laser was used to pump another dye laser (Sirah, PESC-G-24) which operated at $\lambda = 537.671$ nm (~8–10 mJ).

The detection of $O(^1S_0)$ atoms was also via the autoionization method, but at 121.765 nm for the $O^*[2s^22p^3(^2P^\circ)3s\ (^1P^\circ_1)] \leftarrow O(^1S_0)$ transition.[73] The 121.765 nm laser was generated by the resonant difference-frequency ($2\omega'_1 - \omega'_2$) four-wave mix-

26 September 2024 02:50:31

Published under an exclusive license by AIP Publishing

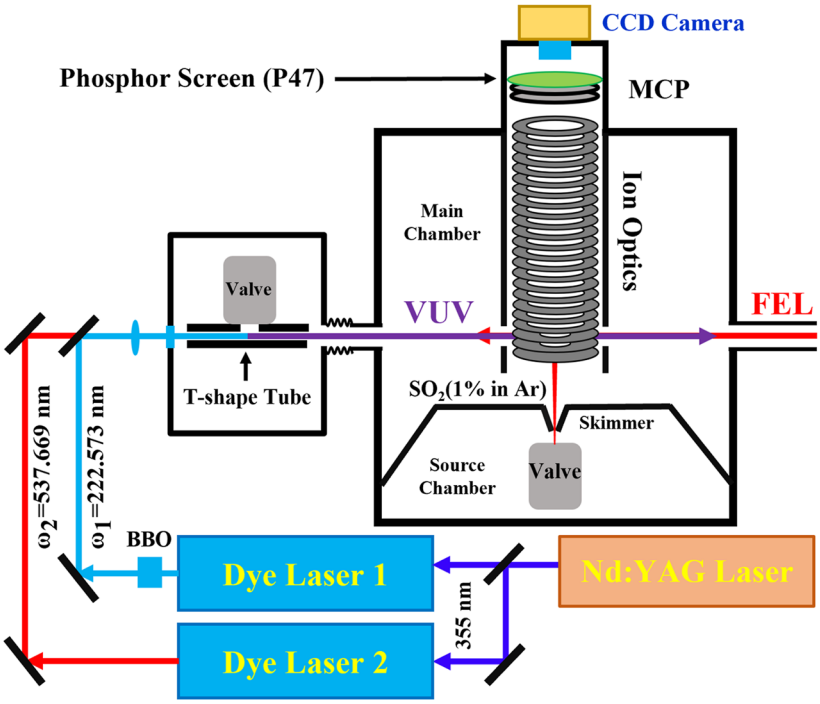

FIG. 2. Schematic view of the VUV pump–VUV probe combined with the time-sliced velocity map ion imaging experimental setup.

ing (DFWM) method in the Kr/Ar mixture (volume ratio = 1:3), in which ω'_1 was set at 212.556 nm corresponding to the two-photon resonant frequency for the Kr $[4s^24p^5(^2P_{3/2})5p\ ^2[1/2]_0 \leftarrow 4s^24p^6\ ^1S_0]$ transition. In order to guarantee equal detection sensitivity of all product velocities, ω'_2 was also scanned back and forth equally around 835.671 nm to cover the Doppler profile. The light at λ = 212.556 nm (~1 mJ) was produced by doubling the output of a dye laser (Sirah, PESC-G-24) operating at λ ~ 425 nm, which was pumped by the 355 nm Nd:YAG laser (Continuum PL-9030). The 532 nm output of the same Nd:YAG laser was used to pump another dye laser (Sirah, PESC-G-24) to obtain ω'_2 at λ = 835.671 nm (~8–10 mJ). To avoid the $O(^1S_0)$ atom from the secondary dissociation, an off-axis biconvex LiF lens was applied to disperse the 212.556 nm light from the direction of 121.765 nm beam.

The 1% SO_2 was seeded in Ar and expanded into the source chamber by a general valve. The supersonic molecular beam entered the ion optics assembly[74] (23-plate ion optics) after running through a skimmer (mounted between the source chamber and the reaction chamber) and a 2 mm hole in the first electrode and then propagated along the center axis of the ion optics assembly equipped in the reaction chamber. The molecular beam was intersected perpendicularly by the photolysis and probe lasers between the second and third plates of the ion optics assembly. The $O(^1D_2)/O(^1S_0)$ photoproducts from the photodissociation of SO_2 by the VUV-FEL were subsequently probed by one photon excitation at λ = 92.201 or 121.765 nm; the resulting O^+ ions were accelerated through the remaining ion optics and detected by a dual microchannel plate (MCP) detector coupled with a P47 phosphor screen. In the current experiments, the detector was gated to select m/z = 16 with a pulse width of about 20 ns. The signals exclusively from one of the VUV laser beams were quite small and have been subtracted from the two-color VUV pump–VUV probe signals. The relative timings of the pulsed molecular beam, the pump and probe lasers, the detector gate pulse, and the CCD camera were controlled by two digital delay generators (DG645, Stanford Research Systems), and the typical delay between the photodissociation and photoionization laser beams was in the range of 10–20 ns. The speed of the product was calibrated using the O^+ signal from the photodissociation of O_2 at 225.0 nm.[74,75]

III. RESULTS AND DISCUSSIONS

A. The $O(^1D_2)$ + SO ($X^3\Sigma^-$, $a^1\Delta$, $b^1\Sigma^+$) photoproduct channels

1. The raw images and corresponding total kinetic energy release distributions

The $O(^1D_2)$ product ion images from SO_2 photodissociation have been recorded at six wavelengths shown by red downward arrows in Fig. 1, namely, 131.0, 127.1, 125.9, 125.2, 124.4, and 121.6 nm, and the corresponding raw images are shown in Fig. 3. In these images, the electric vectors of the dissociation and ionization lasers are pointing in the same direction, i.e., parallel to the face of the microchannel plate detector, which are shown as the double headed red arrow in Fig. 3. The velocity of the $O(^1D_2)$ product has been measured by the time-sliced velocity map ion imaging method.[74,75] In the center-of-mass frame, the conservation

26 September 2024 02:50:31

Published under an exclusive license by AIP Publishing

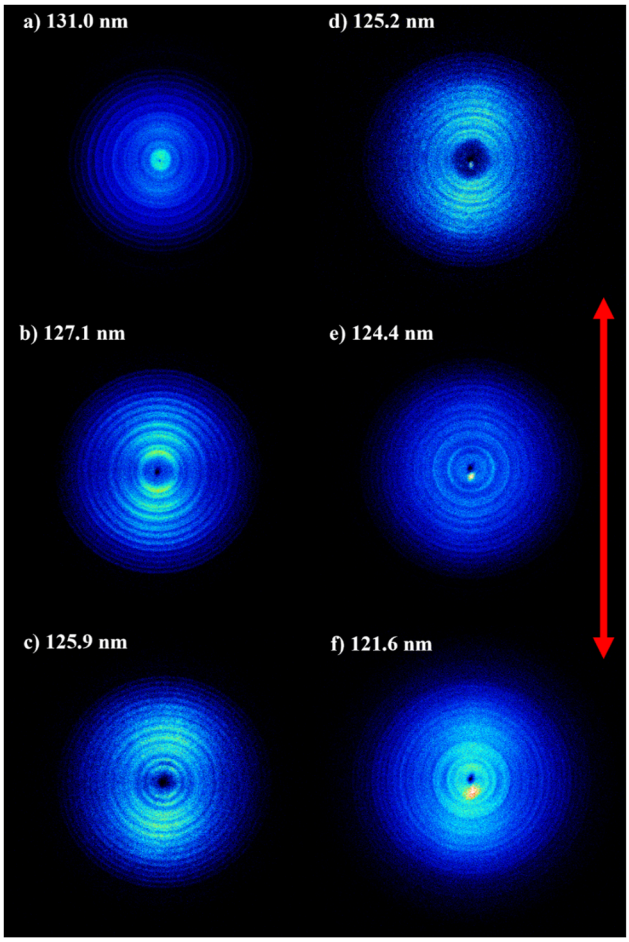

FIG. 3. Raw images of the $O(^1D_2)$ atoms produced in the photodissociation of SO_2 after excitation by the VUV lasers at (a) 131.0 nm, (b) 127.1 nm, (c) 125.9 nm, (d) 125.2 nm, (e) 124.4 nm, and (f) 121.6 nm. The double headed red arrow represents the polarization direction of the photolysis laser.

of momentum is tenable during the photodissociation process; we have

$$m_{O(^1D_2)} v_{O(^1D_2)} = m_{SO} v_{SO}, \quad (1)$$

where m and v represent the mass and velocity of photofragments as shown in the subscript, respectively. Thus, the total kinetic energy of $O(^1D_2)$ and SO photofragments can be written as

$$E_T = \frac{1}{2} m_{O(^1D_2)} v^2_{O(^1D_2)} + \frac{1}{2} m_{SO} v^2_{SO} = \frac{1}{2} \frac{m_{SO_2}}{m_{SO}} m_{O(^1D_2)} v^2_{O(^1D_2)}. \quad (2)$$

According to the law of conservation of energy, the vibrational level of the SO fragment is related to the translational energy,

$$E_T = h\nu - D_0(SO - O) - E_{O(^1D_2)} - E_{SO}, \quad (3)$$

where $h\nu$ is the photon energy, $D_0(SO–O)$ is the SO_2 dissociation energy, 45 725.3 ± 0.1 cm^{-1}, to form $SO(\tilde{X}^3\Sigma^-) + O(^3P_2)$.[9] $E_{O(^1D_2)}$ is the internal energy of the $O(^1D_2)$ atom, which is constant with a value of 15 867.862 cm^{-1}, and E_{SO} is the SO internal energy. The total kinetic energy release distributions (TKERs) extracted from the images are shown in Fig. 4, which are obtained by integrating the signals of the image over the full angular range. Based on Eq. (3) and the term values of the SO energy levels,[76] the well-resolved structures in the TKERs have been assigned to the vibrational levels of the $SO(X^3\Sigma^-)$, $SO(a^1\Delta)$, and $SO(b^1\Sigma^+)$ products, which are marked by orange, blue, and green drop lines, respectively.

Obviously, the spin-allowed dissociation channel $O(^1D_2)$ + $SO(a^1\Delta)$ is dominant because of the excellent agreement between the energy threshold of this channel and the onset of the signals for all experimental wavelengths. The spin-forbidden channel $O(^1D_2)$ + $SO(X^3\Sigma^-)$ seems to be minor by reason of the absent signals from its energy threshold to the onset of the $O(^1D_2)$ + $SO(a^1\Delta)$ channel in the TKERs. However, when we check the assignments of $SO(a^1\Delta)$ vibrational structures carefully, which become more and more mismatched with the increase in vibrational quantum numbers, in particular, the vibrational structures become bimodal in the region of TKER ≤ 5000 cm^{-1}, which requires further analysis to the assignments of these vibrational structures. The $SO(b^1\Sigma^+)$ products should be taken into account due to its appropriate energy threshold; however, the vibrational levels of $SO(b^1\Sigma^+)$ do not match well with the bimodal vibrational structures in the low TKER region. Thus, we have to consider the vibrational levels of $SO(X^3\Sigma^-)$. Indeed, the onset of each vibrational level of $SO(X^3\Sigma^-)$ product is in excellent agreement with the right profile of the bimodal structure. Therefore, the spin-forbidden channel $O(^1D_2)$ + $SO(X^3\Sigma^-)$ should be present, with the $SO(X^3\Sigma^-)$ products being highly vibrationally excited.

To obtain information on the product state distributions, a systematic approach was used to extract the SO(v, N) distributions from each $O(^1D_2)$ image. A homemade software application was used to fit the TKERs, in which the SO internal energies were calculated according to the reports from Yu and Bian[76] The SO vibration–rotation internal energies were converted into TKER, using the conservation of energy, as shown by the drop lines in Fig. 4. During the simulation of TKERs, the rotational distributions of each SO vibrational state obey the Gaussian distributions as far as possible, and the intensities were varied until the best fit to the experimental data was obtained. The results are shown as red curves in Fig. 4, which are the sum of individual simulated vibrational peaks exhibited as orange, blue, and green dotted lines for $SO(X^3\Sigma^-)$, $SO(a^1\Delta)$, and $SO(b^1\Sigma^+)$, respectively.

In our simulations of the TKERs, the peak of the rotational state populations for each vibrational state is slightly increasing with the increase in the vibrational quantum number and has an average of N ~ 20, corresponding to about 300 cm^{-1} rotational excitation (the rotation temperature of ~400 K), which means that only 1.5% of the available energy is deposited into purely rotational excitation. Such a low rotational excitation ratio indicates that the bond angle of the SO_2 transient structure changes little during the dissociation process.

2. The vibrational distributions and the branching ratios

Integrating the rotational distributions, the vibrational state population distributions of the $SO(X^3\Sigma^-)$, $SO(a^1\Delta)$, and $SO(b^1\Sigma^+)$ products in the $O(^1D_2)$ + SO channels have been obtained and

26 September 2024 02:50:31

Published under an exclusive license by AIP Publishing

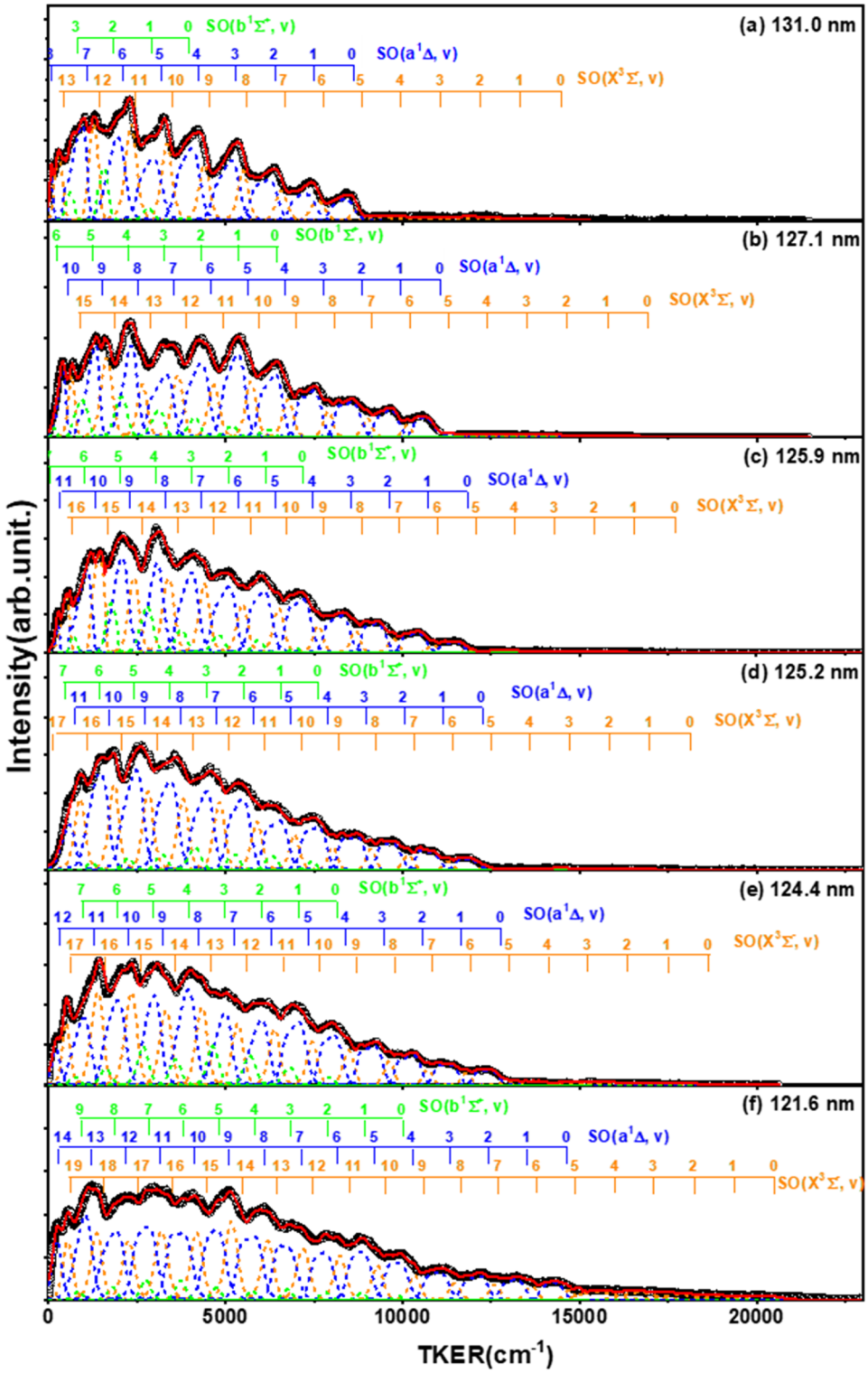

FIG. 4. (a)–(f) Total kinetic energy release (TKER) spectra (black open-circle curves) derived from the raw images shown in Fig. 3. The orange, blue, and green drop lines on the TKER spectra designate the vibrational levels of the SO($X^3\Sigma^-$), SO($a^1\Delta$), and SO($b^1\Sigma^+$) products, respectively. The vibrational state assignments are based on the simulated vibrational distributions (red curves), which represent the sum of individual simulated vibrational peaks (orange, blue, and green dotted lines).

26 September 2024 02:50:31

Published under an exclusive license by AIP Publishing

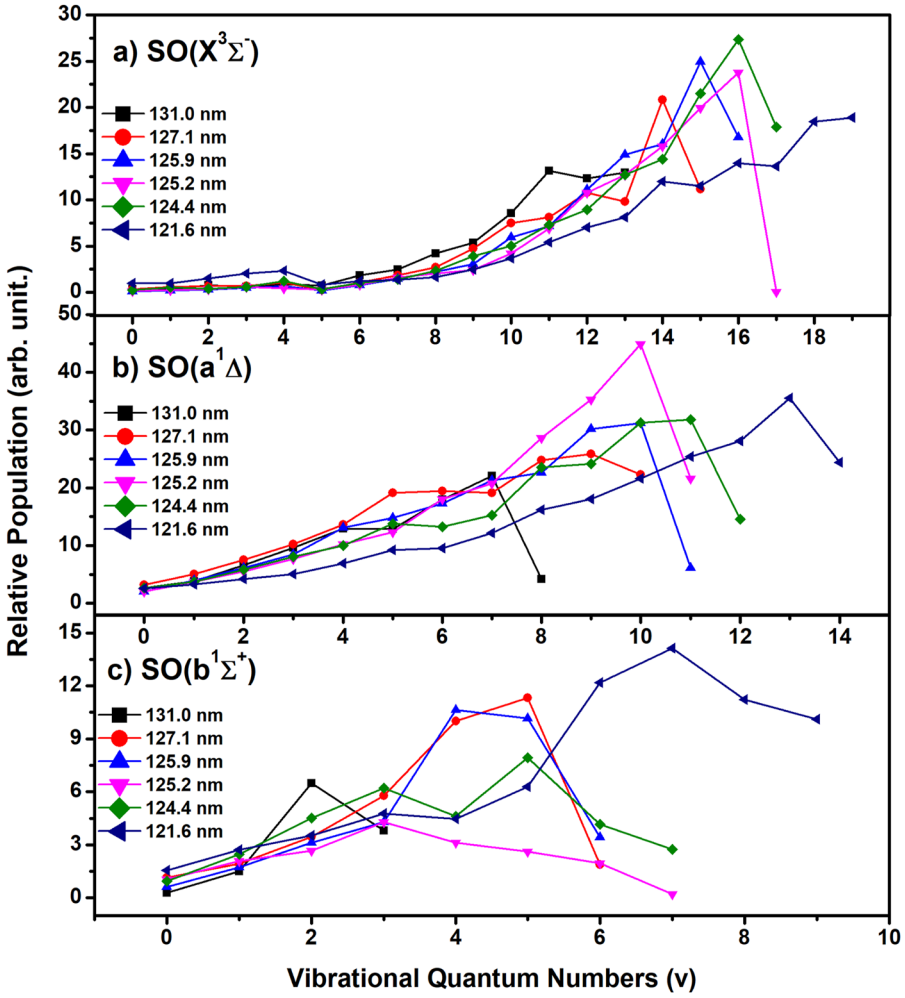

FIG. 5. Vibrational state distributions of the (a) SO($X^3\Sigma^-$), (b) SO($a^1\Delta$), and (c) SO($b^1\Sigma^+$) products in the O($^1D_2$) product channels from the SO_2 photodissociation, extracted from the simulation shown in Fig. 4.

are shown in Fig. 5. The vibrational distributions were found to be inverted, with the population peaking at high vibrational levels close to the energy threshold for each dissociation channel. The same vibrational distributions of the SO($X^3\Sigma^-$), SO($a^1\Delta$), and SO($b^1\Sigma^+$) products indicate that they are probably produced through the similar dynamical mechanisms. The simulations return the branching ratios for the different channels observed in this work. It is clear that the branching ratios show a weak dependence of the photolysis wavelength (Fig. 6). The relative branching ratios for the channels O($^1D_2$) + SO($X^3\Sigma^-$), O($^1D_2$) + SO($a^1\Delta$), and O($^1D_2$) + SO($b^1\Sigma^+$) are determined to be ~0.3, ~0.6, and ~0.1, respectively.

3. Anisotropy parameters

In a molecular photodissociation process, the photodissociation product detected at an angle in the center-of-mass frame relative to the photolysis laser polarization can be represented by the following formula:[77]

$$\psi(E_T, \theta) = \sigma(E_T)\{1 + \beta(E_T)P_2(\cos\theta)\}, \quad (4)$$

where $\sigma(E_T)$ is the product translational energy distribution and $\beta(E_T)$ is the energy-dependent anisotropy parameter. θ represents the angle between the direction of the recoil velocity of the dissociative products and the polarization axis of the linearly polarized photolysis laser. $P_2(\cos\theta)$ is the second-order Legendre polynomial.

Angular distributions were obtained for the O($^1D_2$) product channel at six wavelengths by integrating the imaging signals over the radius (Fig. 7). Due to the partial overlap between the vibrational profiles, the vibrational state-dependent anisotropy parameters cannot be extracted from the images exactly; here, we provide the average β values as a function of the photolysis wavelength. By fitting the angular distributions with Eq. (4), the averaged anisotropy parameters over the product velocity distribution are determined to be 0.22, 0.58, 0.57, 0.60, 0.10, and 0.37 at wavelengths of 131.0, 127.1, 125.9, 125.2, 124.4, and 121.6 nm, respectively. Within the error bar,

26 September 2024 02:50:31

Published under an exclusive license by AIP Publishing

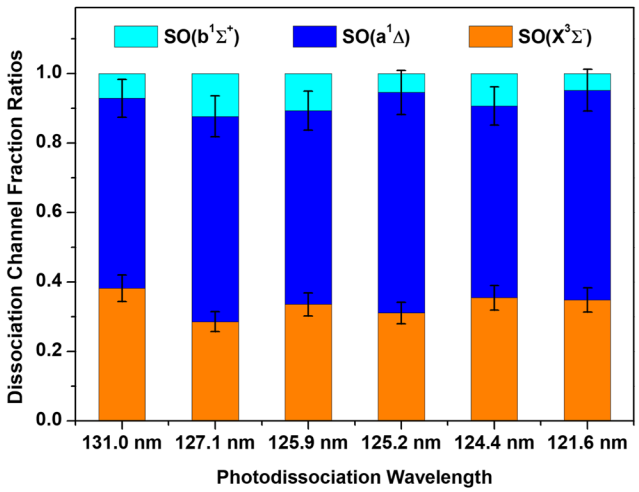

FIG. 6. Branching ratios of SO($X^3\Sigma^-$), SO($a^1\Delta$), and SO($b^1\Sigma^+$) products for the O($^1D_2$) + SO channels at six photolysis wavelengths. The sum of the branching ratios at each photolysis wavelength is normalized to be unity.

these values are all positive and slightly dependent on the wavelength but seem to be irregular. The lowest value of β parameter appears at 124.4 nm with a value of 0.1, which shows an almost isotropic angular distribution and indicates a quite slow dissociation process. The same β parameters of around 0.6 at 127.1, 125.9, and 125.2 nm suggest a relatively fast (compared to rotation) dissociation process from parallel electronic excitation.

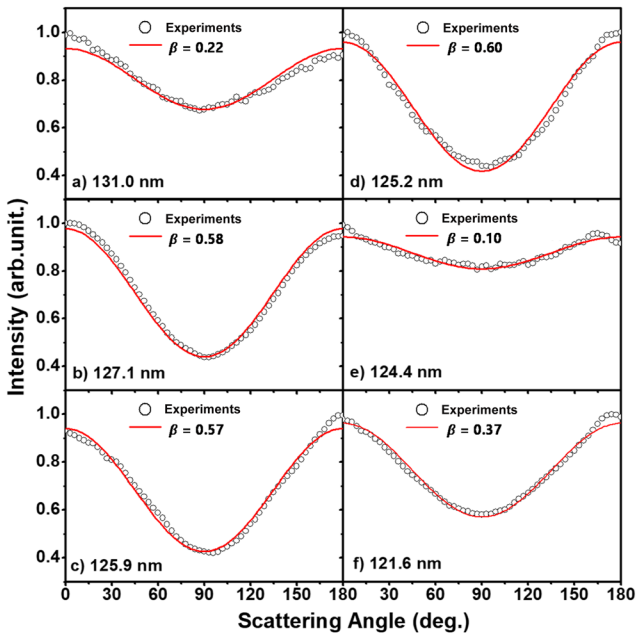

FIG. 7. (a)–(f) Angular distributions obtained for the O($^1D_2$) product channels at six different photolysis wavelengths between 121.6 and 131.0 nm (open dots). A fit (solid line) to the obtained data yields slightly changed anisotropy parameters.

B. The O($^1S_0$) + SO($X^3\Sigma^-$) photoproduct channel

At the Lyman-α wavelength (121.6 nm), the O($^1S_0$) + SO($X^3\Sigma^-$) photoproduct channel is also energetically allowed[11] and has been studied by detecting O($^1S_0$) using the wavelength of 121.765 nm via the $O^*[2s^22p^3(^2P^\circ)3s\ (^1P^\circ_1)] \leftarrow O(^1S_0)$ transition. The raw images and the corresponding TKERs are shown in Fig. 8. A series of structures are observed, and the main peaks match with the onsets of the vibrational states of the SO($X^3\Sigma^-$) products very well. The profiles of the vibrational states indicate that the SO($X^3\Sigma^-$) products may have a bimodal rotational state distribution. The simulation based on the above-mentioned method has been performed, and the relative vibrational state populations of SO($X^3\Sigma^-$) and the β parameters as a function of vibrational states are displayed in Table I. Almost half of the SO($X^3\Sigma^-$) products are populated in the v = 1 vibrational state, illustrating the relatively moderate vibrational excitation of SO($X^3\Sigma^-$) in this dissociation channel. As shown in Table I, the β parameters increase linearly from 0.25 to 0.54 with the vibrational state increasing from v = 0 to v = 2, which suggests that a bent transition state may be involved in the formation of products at higher vibrational states.

C. Dissociation mechanisms

As shown in the inset of Fig. 1, Suto *et al.*[11] measured the fluorescence yields from the photodissociation of SO_2 at 106–133 nm, in which a photoabsorption spectrum with better resolution was obtained and the vibrational progressions were ascribed to the bending vibrational excitation. They assigned the $\tilde{G}$ state to a transition from the $8a_1$ to the 4*s* orbital and provided an A_1 symmetry. Later, the two-photon experiments by Xue *et al.*[63] identified that the transition is, in fact, from the $8a_1$ to 4*p* orbital. This discovery gave three different possibilities for the symmetry of the $\tilde{G}$ state, namely, A_1, B_1, or B_2. According to the calculation by Palmer *et al.*,[21] only one $^1B_1$ Rydberg state originating from 9.674 eV (128.159 nm) exists in this energy range, which is in excellent agreement with the origin of the $\tilde{G}$ state (9.768 eV).[11] In addition, the $\tilde{G}$ band contains a complex shoulder; Palmer *et al.*[21] denoted it as $\tilde{G}'$. However, the $\tilde{G}$ state and its shoulder ($\tilde{G}'$) have the same vibrational progression of frequency ~380 cm^{-1}[11] and the same dissociation dynamics (this work); all these make us believe that this shoulder is the extend of the $\tilde{G}$ state rather than a new electronically excited state. Thus, our experimental wavelengths mainly concentrate on the bending vibrational excitation of the $\tilde{G}^1B_1$ state except for 131.0 nm, which located in the $\tilde{F}$ Rydberg state (originate from 9.1832 eV, 135.009 nm).[21]

The present work provides a state-resolved picture of the primary photochemical processes O($^1D_2$) + SO($X^3\Sigma^-$, $a^1\Delta$, $b^1\Sigma^+$) after the excitation of SO_2 into the $\tilde{G}$ state. The non-selectivity (with respect to electron spin) suggests that the potential energy surface crossings and strong spin–orbit coupling are effective. However, the detailed dissociation mechanism is hard to illustrate clearly due to the absence of PESs of the high-lying electronic states as well as the complex couplings between the PESs. Tokue and Nanbu[20] and Katagiri *et al.*[16] calculated the potential energy curves of $SO_2 \rightarrow$ SO + O($^3P/^1D$) and illuminated that there are three $^1A'$ states and two $^1A''$ states correlating with the O($^1D_2$) + SO($b^1\Sigma^+$) channel, five $^1A'$ states and five $^1A''$ states correlating with the O($^1D_2$) + SO($a^1\Delta$) channel, and two $^3A'$ states and three $^3A''$ states correlating with the O($^1D_2$) + SO($X^3\Sigma^-$) channel.

26 September 2024 02:50:31

Published under an exclusive license by AIP Publishing

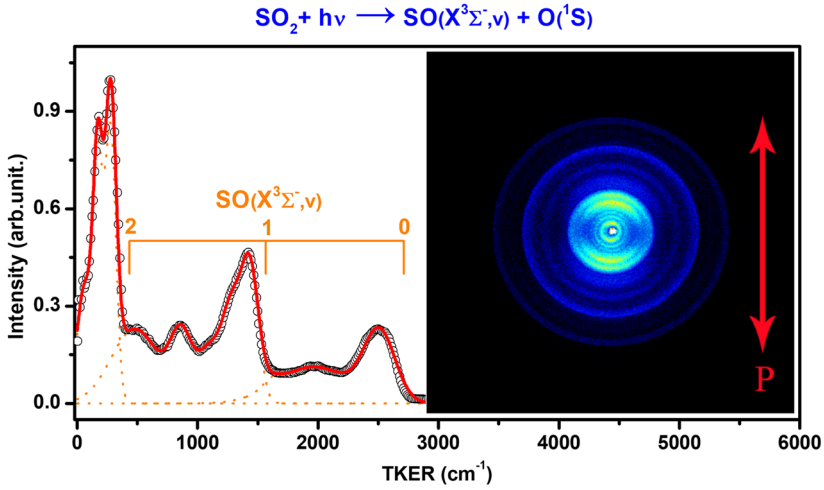

FIG. 8. Time-sliced velocity map ion images for $O(^1S_0)$ photofragments from SO_2 photodissociation recorded at 121.765 nm and its corresponding TKER spectra. The orange drop lines on the TKER spectra designate the vibrational levels of the $SO(X^3\Sigma^-)$ products. The vibrational state assignments are based on the simulated vibrational distributions (red line), which represents the sum of individual simulated vibrational peaks (orange dotted lines).

For instance, theoretical calculations[33] suggested that the $3^1A'$ state is quasi-bound but has an avoided crossing with $4^1A'$, which lies only ~0.5 eV higher in energy, leading to the $3^1A'$ state being dissociative and correlating with the ground state $SO(X^3\Sigma^-) + O(^3P)$ dissociation channel, while the avoided crossing leads the $4^1A'$ state to correlate with the $O(^1D_2) + SO(a^1\Delta)$ dissociation channel. Meanwhile, the $2^1A'$ state originally correlates with $O(^1D_2) + SO(a^1\Delta)$, but it exhibits the crossing seams with the repulsive singlet $3^1A'$ and triplet $2^3A'$ states in the long bond length region, which gives rise to the electronically ground state $SO(X^3\Sigma^-) + O(^3P)$ products. However, Katagiri *et al.*[16] concluded that the interaction between the $2^1A'$ state and the singlet or triplet states occurs around a narrow energy region and is very weak. At a high excitation energy, dissociation through the $2^1A'$ state should lead to $O(^1D_2) + SO(a^1\Delta)$ products. No experimental signals for $O(^3P) + SO(X^3\Sigma^-)$ channels observed in this work confirm this assumption. In addition, the $3^1A''$ and $2^1A''$ states also adiabatically lead to the $O(^1D_2) + SO(a^1\Delta)$ dissociation channel.

Thus, the initial excited SO_2 molecules to the $\tilde{G}$ state may couple to the singlet low-lying electronic states, like the $4^1A'$, $3^1A''$, and $2^1A'$ state, by multistep internal conversions, and then dissociate on these low-lying states, leading to the $O(^1D_2) + SO(a^1\Delta)$ dissociation channel. In addition, the singlet states such as $3^1A''$ and $4^1A'$ may further cross with several repulsive triplet states along the dissociation coordinate by intersystem crossings and generate electronically ground state $SO(X^3\Sigma^-)$ products. The $O(^1D_2) + SO(b^1\Sigma^+)$ channel has more complicated dissociation mechanisms, and no further discussion is given here without the detailed PES information. The high vibrational excitation and cold rotational excitation of SO products observed in this work demonstrate that the S–O bond of SO_2 is stretched extremely and the bond angle of O–S–O changes little during dissociation. The photon at 131.0 nm excites the SO_2 molecules to the $\tilde{F}$ state, and the dissociation on this state has the same dynamical picture with the $\tilde{G}$ state, suggesting that highly excited SO_2 has common dissociation dynamics, i.e., undergoing multistep internal conversions to low-lying states, and then dissociates on low-lying states.

TABLE I. Relative vibrational state populations of $SO(X^3\Sigma^-)$ and the vibrational state dependences of the β parameters for the $O(^1S_0)$ product channel observed in the photodissociation of SO_2 at 121.765 nm.

$SO(X^3\Sigma^-, v)$	v = 0	v = 1	v = 2
Relative populations	0.23	0.46	0.31
β Parameters	0.25	0.43	0.54

As for the $O(^1S_0) + SO(X^3\Sigma^-)$ product channel, only one wavelength is investigated due to its high energy threshold, and the TKER exhibits the bimodal rotational state distributions of each vibrational state, indicating that there may be two different dissociation pathways. In addition, the v = 0 products have a nearly isotropic angular distribution, while the v = 2 products have obvious anisotropy, illustrating the complex nature of the photodissociation mechanism of SO_2 in the VUV region. The detailed dissociation mechanism still awaits further theoretical investigations.

The SO molecules are widely observed in the ISM and regarded as the production from SO_2 photochemistry.[39,78–81] In this work, the SO molecules from the photodissociation of SO_2 in the VUV region are substantially electronically and rovibrationally excited, which means that these species are highly reactive. Thus, the production of $O(^1D_2/^1S_0)$ atoms and SO radicals from the VUV irradiation of SO_2 could be an important driver in the evolution of the earliest atmosphere.

IV. CONCLUSIONS

In this study, the photodissociation of SO_2 molecule via the $\tilde{G}$ state has been investigated by using the VUV pump–VUV probe

26 September 2024 02:50:31

Published under an exclusive license by AIP Publishing

combined with the time-sliced velocity map ion imaging apparatus. The $O(^1D_2)$ + SO and $O(^1S_0)$ + SO dissociation channels were measured. The branching ratios for $O(^1D_2)$ + $SO(X^3\Sigma^-)$, $O(^1D_2)$ + $SO(a^1\Delta)$, and $O(^1D_2)$ + $SO(b^1\Sigma^+)$ have been derived from the simulation of TKERs and determined to be ~0.3, ~0.6, and ~0.1. The initial excited SO_2 molecules should couple to the low-lying singlet electronic states by multistep internal conversions and mainly produce the $O(^1D_2)$ + $SO(a^1\Delta)$ products. The intersystem crossings between the singlet states and triplet states cause some SO_2 molecules dissociating via the repulsive triplet PESs to produce $O(^1D_2)$ + $SO(X^3\Sigma^-)$. We hope that this work can stimulate further theoretical calculations to demonstrate the dissociation mechanism.

ACKNOWLEDGMENTS

This experimental work was supported by the National Natural Science Foundation of China (Grant Nos. 22241304, 22225303, and 22173082), the National Natural Science Foundation of China [NSFC Center for Chemical Dynamics (Grant No. 22288201)], the Scientific Instrument Developing Project of the Chinese Academy of Sciences (Grant No. GJJSTD20220001), and the Innovation Program for Quantum Science and Technology (Grant No. 2021ZD0303304). X. Yang also acknowledges the Guangdong Science and Technology Program (Grant Nos. 2019ZT08L455 and 2019JC01X091), and the Shenzhen Science and Technology Program (Grant No. ZDSYS20200421111001787).

AUTHOR DECLARATIONS

Conflict of Interest

The authors have no conflicts to disclose.

Author Contributions

Y.W., J.S., and Z.L. contributed equally to this work.

Yucheng Wu: Data curation (equal); Formal analysis (equal); Methodology (equal); Validation (equal); Writing – original draft (equal); Writing – review & editing (equal). **Jitao Sun**: Data curation (equal); Formal analysis (equal); Methodology (equal); Validation (equal); Writing – original draft (equal); Writing – review & editing (equal). **Zhenxing Li**: Data curation (equal); Formal analysis (equal); Methodology (equal); Validation (equal); Writing – original draft (equal); Writing – review & editing (equal). **Zhaoxue Zhang**: Data curation (supporting); Methodology (supporting); Validation (supporting); Writing – review & editing (supporting). **Zijie Luo**: Data curation (supporting); Formal analysis (supporting); Methodology (supporting); Validation (supporting); Writing – review & editing (supporting). **Yao Chang**: Data curation (equal); Formal analysis (supporting); Validation (equal); Writing – original draft (lead); Writing – review & editing (supporting). **Guorong Wu**: Data curation (supporting); Formal analysis (supporting); Methodology (supporting); Writing – review & editing (supporting). **Weiqing Zhang**: Formal analysis (supporting); Methodology (supporting); Validation (supporting); Writing – review & editing (supporting). **Shengrui Yu**: Formal analysis (equal); Funding acquisition (supporting); Methodology (supporting); Validation (supporting); Writing – original draft (supporting); Writing – review & editing (equal). **Kaijun Yuan**: Formal analysis (equal); Funding acquisition (lead); Methodology (supporting); Validation (supporting); Writing – original draft (supporting); Writing – review & editing (lead). **Xueming Yang**: Formal analysis (supporting); Funding acquisition (supporting); Validation (supporting); Writing – review & editing (supporting).

DATA AVAILABILITY

The data that support the findings of this study are available from the corresponding authors upon reasonable request.

REFERENCES

[1] H. Okabe, J. Am. Chem. Soc. **93**, 7095 (1971).
[2] M. W. Wilson, M. Rothschild, D. F. Muller, and C. K. Rhodes, J. Chem. Phys. **77**, 1837 (1982).
[3] C. S. Effenhauser, P. Felder, and J. R. Huber, Chem. Phys. **142**, 311 (1990).
[4] B. R. Cosofret, S. M. Dylewski, and P. L. Houston, J. Phys. Chem. A **104**, 10240 (2000).
[5] T. P. Rakitzis, P. C. Samartzis, and T. N. Kitsopoulos, Phys. Rev. Lett. **87**, 123001 (2001).
[6] K. Yamasaki, F. Taketani, K. Sugiura, I. Tokue, and K. Tsuchiya, J. Phys. Chem. A **108**, 2382 (2004).
[7] D. P. Hydutsky, N. J. Bianco, and A. W. Castleman, Chem. Phys. **350**, 212 (2008).
[8] S. Becker, C. Braatz, J. Lindner, and E. Tiemann, Chem. Phys. Lett. **208**, 15 (1993).
[9] S. Becker, C. Braatz, J. Lindner, and E. Tiemann, Chem. Phys. **196**, 275 (1995).
[10] H. Hamdy, Z. X. He, and J. A. R. Samson, J. Phys. B: At., Mol. Opt. Phys. **24**, 4803 (1991).
[11] M. Suto, R. L. Day, and L. C. Lee, J. Phys. B: At., Mol. Opt. Phys. **15**, 4165 (1982).
[12] D. E. Freeman, K. Yoshino, J. R. Esmond, and W. H. Parkinson, Planet. Space Sci. **32**, 1125 (1984).
[13] K. Yamanouchi, M. Okunishi, Y. Endo, and S. Tsuchiya, J. Mol. Struct. **352–353**, 541 (1995).
[14] C. Jaffé, J. Chem. Phys. **81**, 616 (1984).
[15] K. Kamiya and H. Matsui, Bull. Chem. Soc. Jpn. **64**, 2792 (1991).
[16] H. Katagiri, T. Sako, A. Hishikawa, T. Yazaki, K. Onda, K. Yamanouchi, and K. Yoshino, J. Mol. Struct. **413–414**, 589 (1997).
[17] T. Sako, A. Hishikawa, and K. Yamanouchi, Chem. Phys. Lett. **294**, 571 (1998).
[18] O. Bludsky, P. Nachtigall, J. Hrusak, and P. Jensen, Chem. Phys. Lett. **318**, 607 (2000).
[19] D. Xie, G. Ma, and H. Guo, J. Phys. Chem. A **111**, 7782 (1999).
[20] I. Tokue and S. Nanbu, J. Chem. Phys. **132**, 024301 (2010).
[21] M. H. Palmer, D. A. Shaw, and M. F. Guest, Mol. Phys. **103**, 1183 (2005).
[22] P. J. Singh, A. Shastri, R. D'Souza, S. V. N. Bhaskara Rao, and B. N. Jagatap, J. Quant. Spectrosc. Radiat. Transfer **113**, 267 (2012).
[23] C. Xie, X. Hu, L. Zhou, D. Xie, and H. Guo, J. Chem. Phys. **139**, 014305 (2013).
[24] C. Lévêque, R. Taïeb, and H. Köppel, Chem. Phys. Lett. **460**, 135 (2015).
[25] J. Jiang, G. B. Park, and R. W. Field, J. Chem. Phys. **144**, 144312 (2016).
[26] H. Ran, D. Xie, and H. Guo, Chem. Phys. Lett. **439**, 280 (2007).
[27] S. O. Danielache, C. Eskebjerg, M. S. Johnson, Y. Ueno, and N. Yoshida, J. Geophys. Res. **113**, D17314 (2008).
[28] C. Xie, B. Jiang, J. Klos, P. Kumar, M. H. Alexander, B. Poirier, and H. Guo, J. Phys. Chem. A **121**, 4930 (2017).
[29] X. Huang, D. W. Schwenke, and T. J. Lee, J. Chem. Phys. **140**, 114311 (2014).
[30] C. Leveque, R. Taieb, and H. Koppel, J. Chem. Phys. **140**, 091101 (2014).
[31] S. Mai, P. Marquetand, and L. Gonzalez, J. Chem. Phys. **140**, 204302 (2014).

26 September 2024 02:50:31

Published under an exclusive license by AIP Publishing

[32]J. Klos, M. H. Alexander, P. Kumar, B. Poirier, B. Jiang, and H. Guo, J. Chem. Phys. **144**, 174301 (2016).
[33]J. Jiang, G. B. Park, and R. W. Field, J. Chem. Phys. **144**, 144313 (2016).
[34]G. B. Park, J. Jiang, C. A. Saladrigas, and R. W. Field, J. Chem. Phys. **144**, 144311 (2016).
[35]P. Kumar and B. Poirier, Mol. Phys. **117**, 2456 (2019).
[36]J. Farquhar, J. Savarino, T. L. Jackson, and M. H. Thiemens, Nature **404**, 50 (2000).
[37]R. W. Carlson, R. E. Johnson, and M. S. Anderson, Science **286**, 97 (1999).
[38]A. S. Khayat, G. L. Villanueva, M. J. Mumma, and A. T. Tokunaga, Icarus **253**, 130 (2015).
[39]U. Calmonte, K. Altwegg, H. Balsiger, J. J. Berthelier, A. Bieler, G. Cessateur, F. Dhooghe, E. F. van Dishoeck, B. Fiethe, S. A. Fuselier, S. Gasc, T. I. Gombosi, M. Hässig, L. Le Roy, M. Rubin, T. Sémon, C. Y. Tzou, and S. F. Wampfler, Mon. Not. R. Astron. Soc. **462**, S253 (2016).
[40]R. Dungee, A. Boogert, C. N. DeWitt, E. Montiel, M. J. Richter, A. G. Barr, G. A. S. B. BlakeCharnley, N. Indriolo, A. Karska, D. A. Neufeld, R. L. Smith, A. G. G. M. Tielens, and A. Tielens, Astrophys. J. Lett. **868**, L10 (2018).
[41]X. Zhang, M.-C. Liang, F. Montmessin, J.-L. Bertaux, C. Parkinson, and Y. L. Yung, Nat. Geosci. **3**, 834 (2010).
[42]J. C. Gérard, S. W. Bougher, M. A. López-Valverde, M. Pätzold, P. Drossart, and G. Piccioni, Space Sci. Rev. **212**, 1617 (2017).
[43]S. Kumar, Nature **280**, 758 (1979).
[44]J. Pearl, R. Hanel, V. Kunde, W. Maguire, K. Fox, S. Gupta, C. Ponnamperuma, and F. Raulin, Nature **280**, 755 (1979).
[45]B. A. Smith, E. M. Shoemaker, S. W. Kieffer, and A. F. Cook, Nature **280**, 738 (1979).
[46]M. H. Carr, Nature **313**, 735 (1985).
[47]D. Golomb, K. Watanabe, and F. F. Marmo, J. Chem. Phys. **36**, 958 (1962).
[48]I. W. Watkins, J. Mol. Spectrosc. **29**, 402 (1969).
[49]S. L. Manatt and A. L. Lane, J. Quant. Spectrosc. Radiat. Transfer **50**, 267 (1993).
[50]D. M. P. Holland, D. A. Shaw, and M. A. Hayes, Chem. Phys. **201**, 299 (1995).
[51]C. Leveque, A. Komainda, R. Taieb, and H. Koppel, J. Chem. Phys. **138**, 044320 (2013).
[52]H. B. Franz, S. O. Danielache, J. Farquhar, and B. A. Wing, Chem. Geol. **362**, 56 (2013).
[53]J. Farquhar, H. Bao, and M. Thiemens, Science **289**, 756 (2000).
[54]F. Gaillard, B. Scaillet, and N. T. Arndt, Nature **478**, 229 (2011).
[55]A. R. Whitehill, C. Xie, X. Hu, D. Xie, H. Guo, and S. Ono, Proc. Natl. Acad. Sci. U. S. A. **110**, 17697 (2013).
[56]R. Shaheen, M. M. Abaunza, T. L. Jackson, J. McCabe, J. Savarino, and M. H. Thiemens, Proc. Natl. Acad. Sci. U. S. A. **111**, 11979 (2014).
[57]T. Sato, T. Kinugawa, T. Arikawa, and M. Kawasaki, Chem. Phys. **165**, 173 (1992).
[58]C. Braatz and E. Tiemann, Chem. Phys. **229**, 93 (1998).
[59]N. Hansen, U. Andresen, H. Dreizler, J. U. Grabow, H. Mäder, and F. Temps, Chem. Phys. Lett. **289**, 311 (1998).
[60]M. Brouard, R. Cireasa, A. P. Clark, T. J. Preston, C. Vallance, G. C. Groenenboom, and O. S. Vasyutinskii, J. Phys. Chem. A **108**, 7965 (2004).
[61]J. H. Clements, Phys. Rev. **47**, 224 (1935).
[62]V. Svoboda, N. B. Ram, R. Rajeev, and H. J. Worner, J. Chem. Phys. **146**, 084301 (2017).
[63]B. Xue, Y. Chen, and H.-L. Dai, J. Chem. Phys. **112**, 2210 (2000).
[64]Z. Li, M. Zhao, T. Xie, Y. Chang, Z. Luo, Z. Chen, X. Wang, K. Yuan, and X. Yang, Mol. Phys. **119**, e1813911 (2020).
[65]J. Zhou, Y. Zhao, C. S. Hansen, J. Yang, Y. Chang, Y. Yu, G. Cheng, Z. Chen, Z. He, S. Yu, H. Ding, W. Zhang, G. Wu, D. Dai, C. M. Western, M. N. R. Ashfold, K. Yuan, and X. Yang, Nat. Commun. **11**, 1547 (2020).
[66]Z. Li, M. Zhao, T. Xie, Z. Luo, Y. Chang, G. Cheng, J. Yang, Z. Chen, W. Zhang, G. Wu, X. Wang, K. Yuan, and X. Yang, J. Phys. Chem. Lett. **12**, 844 (2021).
[67]Y. Zhao, Z. Luo, Y. Chang, Y. Wu, S.-e. Zhang, Z. Li, H. Ding, G. Wu, J. S. Campbell, C. S. Hansen, S. W. Crane, C. M. Western, M. N. R. Ashfold, K. Yuan, and X. Yang, Nat. Commun. **12**, 4459 (2021).
[68]Y. Song, H. Gao, C. Ng, W. Jackson, W. M. Jackson, C. Joblin, and L. d'Hendecourt, EAS Publ. Ser. **58**, 295 (2013).
[69]H. Gao, Y. Song, W. M. Jackson, and C. Y. Ng, J. Chem. Phys. **138**, 191102 (2013).
[70]C. Y. Ng, Annu. Rev. Phys. Chem. **65**, 197 (2014).
[71]Y. Chang, S. Yu, Q. Li, Y. Yu, H. Wang, S. Su, Z. Chen, L. Che, X. Wang, W. Zhang, D. Dai, G. Wu, K. Yuan, and X. Yang, Rev. Sci. Instrum. **89**, 063113 (2018).
[72]L. Yu, M. Babzien, I. I. Ben-Zvi, L. F. DiMauro, A. Doyuran, W. Graves, E. Johnson, S. Krinsky, R. Malone, I. I. Pogorelsky, J. Skaritka, G. Rakowsky, L. Solomon, X. J. Wang, M. Woodle, V. V. Yakimenko, S. G. Biedron, J. N. Galayda, E. Gluskin, J. Jagger, V. V. Sajaev, and I. I. Vasserman, Science **289**, 932 (2000).
[73]K. Butler and C. J. Zeippen, J. Phys. IV **01**, C1-141 (1991).
[74]J. J. Lin, J. Zhou, W. Shiu, and K. Liu, Rev. Sci. Instrum. **74**, 2495 (2003).
[75]D. H. Parker and A. T. J. B. Eppink, J. Chem. Phys. **107**, 2357 (1997).
[76]L. Yu and W. Bian, J. Comput. Chem. **32**, 1577 (2011).
[77]R. N. Zare, Mol. Photochem. **4**(1), 1–37 (1972).
[78]F. F. S. van der Tak, A. M. S. Boonman, R. Braakman, and E. F. van Dishoeck, Astron. Astrophys. **412**, 133 (2003).
[79]J. Boissier, D. Bockelée-Morvan, N. Biver, J. Crovisier, D. Despois, B. G. Marsden, and R. Moreno, Astron. Astrophys. **475**, 1131 (2007).
[80]H. Kim, F. Wyrowski, K. M. Menten, and L. Decin, Astron. Astrophys. **516**, A68 (2010).
[81]D. A. Belyaev, F. Montmessin, J.-L. Bertaux, A. Mahieux, A. A. Fedorova, O. I. Korablev, E. Marcq, Y. L. Yung, and X. Zhang, Icarus **217**, 740 (2012).

26 September 2024 02:50:31

Published under an exclusive license by AIP Publishing